Beta/gamma and alpha backgrounds in CRESST-II Phase 2

To cite this article: R. Strauss *et al* JCAP06(2015)030

View the article online for updates and enhancements.

Related content

Recent citations

IOP Astronomy ebooks

Part of your publishing universe and your first choice for astronomy, astrophysics, solar physics and planetary science ebooks.

iopscience.org/books/aas

Beta/gamma and alpha backgrounds in CRESST-II Phase 2

R. Strauss,[a,1] **G. Angloher,**[a] **A. Bento,**[c] **C. Bucci,**[d] **L. Canonica,**[d]
A. Erb,[b,e] **F.v. Feilitzsch,**[b] **N. Ferreiro Iachellini,**[a] **P. Gorla,**[d]
A. Gütlein,[f,g] **D. Hauff,**[a] **J. Jochum,**[h] **M. Kiefer,**[a] **H. Kluck,**[f,g]
H. Kraus,[i] **J.-C. Lanfranchi,**[b] **J. Loebell,**[h] **A. Münster,**[b]
F. Petricca,[a] **W. Potzel,**[b] **F. Pröbst,**[a] **F. Reindl,**[a] **S. Roth,**[b]
K. Rottler,[h] **C. Sailer,**[h] **K. Schäffner,**[d] **J. Schieck,**[f,g] **S. Scholl,**[h]
S. Schönert,[b] **W. Seidel,**[a] **M.v. Sivers,**[b,2] **L. Stodolsky,**[a]
C. Strandhagen,[h] **A. Tanzke,**[a] **M. Uffinger,**[h] **A. Ulrich,**[b] **I. Usherov,**[h]
S. Wawoczny,[b] **M. Willers,**[b] **M. Wüstrich**[a] **and A. Zöller**[b]

[a]Max-Planck-Institut für Physik,
 D-80805 München, Germany
[b]Physik-Department, Technische Universität München,
 D-85748 Garching, Germany
[c]CIUC, Departamento de Fisica, Universidade de Coimbra,
 P3004 516 Coimbra, Portugal
[d]INFN, Laboratori Nazionali del Gran Sasso,
 I-67010 Assergi, Italy
[e]Walther-Meißner-Institut für Tieftemperaturforschung,
 D-85748 Garching, Germany
[f]Institut für Hochenergiephysik der Österreichischen Akademie der Wissenschaften,
 A-1050 Wien, Austria
[g]Atominstitut, Vienna University of Technology,
 A-1020 Wien, Austria
[h]Physikalisches Institut, Eberhard-Karls-Universität Tübingen,
 D-72076 Tübingen, Germany
[i]Department of Physics, University of Oxford,
 Oxford OX1 3RH, United Kingdom

 E-mail: strauss@mpp.mpg.de

---

[1]Corresponding author.
[2]Present address: Albert Einstein Center for Fundamental Physics, University of Bern, CH-3012 Bern,
Switzerland.

Abstract. The experiment CRESST-II aims at the detection of dark matter with scintillating CaWO$_4$ crystals operated as cryogenic detectors. Recent results on spin-independent WIMP-nucleon scattering from the CRESST-II Phase 2 allowed to probe a new region of parameter space for WIMP masses below $3\,\mathrm{GeV/c^2}$. This sensitivity was achieved after background levels were reduced significantly. We present extensive background studies of a CaWO$_4$ crystal, called TUM40, grown at the Technische Universität München. The average beta/gamma rate of $3.51/[\mathrm{kg\,keV\,day}]$ (1-40 keV) and the total intrinsic alpha activity from natural decay chains of $3.08 \pm 0.04\,\mathrm{mBq/kg}$ are the lowest reported for CaWO$_4$ detectors. Contributions from cosmogenic activation, surface-alpha decays, external radiation and intrinsic alpha/beta emitters are investigated in detail. A Monte-Carlo based background decomposition allows to identify the origin of the majority of beta/gamma events in the energy region relevant for dark matter search.

Contents

1 Introduction

During the last two decades, the sensitivity of experiments aiming for the direct detection of particle dark matter [1] in form of weakly interacting massive particles (WIMPs) [2] has been constantly improved. For the spin-independent WIMP-nucleon cross section impressive sensitivities were reached: currently the liquid-xenon based LUX [3] experiment reports the best upper limit ($7.6 \cdot 10^{-10}$ pb at $33 \, \text{GeV}/c^2$). A variety of experiments with different techniques [4] have been operated, however, the results are not consistent. A few experiments [5–7], among which is CRESST-II (Cryogenic Rare Event Search with Superconducting Thermometers) [8], reported a signal excess which is not compatible with limits by other dark matter searches [9–12]. Data from a re-analysis of the commissioning run of CRESST-II [13] showed slight tension with a WIMP interpretation of CRESST-II data and, recently, the first data of CRESST-II Phase 2 [8] suggest a background origin of the excess.

The improvement in sensitivity of CRESST-II detectors has been achieved by a significant reduction of backgrounds. In this paper, we present a comprehensive study of the different backgrounds observed in CRESST-II Phase 2 (section 3). The knowledge of the background origin is crucial for future dark matter searches based on the CRESST technology. The Monte-Carlo (MC) based decomposition of the spectrum into different background sources which is presented in section 4 gives an important input for future R&D activities.

2 The detector module TUM40

CRESST-II detectors are based on a two-channel detector readout which is the key feature to discriminate irreducible radioactive backgrounds. CaWO$_4$ crystals of 200-300 g each, equipped with transition-edge-sensors [14], are operated as cryogenic detectors (called phonon detectors) which allow to measure precisely the total deposited energy E of a particle interaction. An excellent energy threshold of $\mathcal{O}(500\,\text{eV})$ and a resolution on a ‰level (at 2.6 keV) were achieved [8, 15]. In addition, the scintillation light output of these crystals is monitored by a cryogenic silicon-on-sapphire detector (called light detector). Since the relative amount
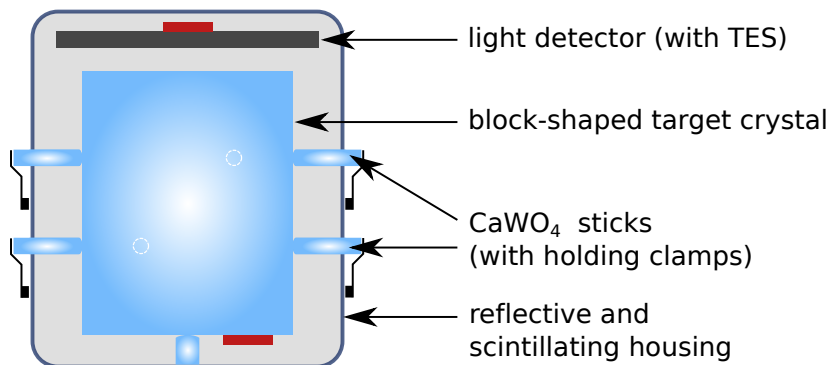
Figure 1. Schematic view of the novel detector module. The block-shaped target crystal TUM40 with a mass of $m = 249\,\mathrm{g}$ is held by $CaWO_4$ sticks. Together with the scintillating polymeric foil the sticks establish a fully scintillating inner detector housing which provides an efficient active veto against surface events. A separate silicon-on-sapphire light detector is installed. For details see [15].

of scintillation light, called light yield (LY),[1] strongly depends on the kind of particle interaction (due to quenching [16]) this channel provides a discrimination of beta/gamma $(LY \sim 1)$, alpha $(LY \sim 0.2)$ and nuclear-recoil events $(LY \lesssim 0.1)$. To a certain extent even O, Ca and W recoils can be distinguished [17]. CRESST uses a unique multi-element target for WIMP search in a single experiment.

Due to a finite resolution of the light channel, the beta/gamma and nuclear-recoil bands overlap in the region-of-interest (ROI) for dark matter search which is typically defined between energy threshold and $40\,\mathrm{keV}$. Several background sources related to surface-alpha decays were identified in the previous run of CRESST-II [18]. In particular ^{206}Pb nuclei from ^{210}Po decays on surrounding surfaces limited the sensitivity. These events appear at low light yields similar to W recoils [15] and are thus indistinguishable from potential WIMP scatters.

However, the decay of ^{210}Po has a corresponding alpha particle with an energy in the MeV-range which is used to reject this background source. Alphas hitting scintillating materials surrounding the $CaWO_4$ crystals produce sufficient additional light to clearly identify a simultaneously occurring recoil of a heavy nucleus.

The crystal investigated in this paper, a block-shaped $CaWO_4$ crystal of $249\,\mathrm{g}$, is mounted in a novel detector module. Instead of (non-scintillating) metal clamps, $CaWO_4$ sticks are used to support the target crystal. The crystal is surrounded by a reflective and scintillating polymeric foil which together with the $CaWO_4$ sticks realizes a detector housing with fully-scintillating inner surfaces. A schematic view of the novel detector design is shown in figure 1, for a detailed description see [15]. As will be presented in section 3.2, this concept provides an efficient rejection of surface-alpha induced Pb-recoils and solves the main background problem of earlier CRESST-II runs [18]. With this detector, a phonon trigger threshold of $\sim 0.60\,\mathrm{keV}$ and a resolution of $\sigma = (0.090 \pm 0.010)\,\mathrm{keV}$ (at $2.60\,\mathrm{keV}$) were achieved [8, 15].

The detector module presented in this paper uses a $CaWO_4$ crystal, called TUM40, grown at the crystal laboratory of the Technische Universität München (TUM) [19]. At this institute, a Czochralski crystal-production facility was set up, dedicated to the growth of $CaWO_4$. The furnace is exclusively used for the CRESST experiment which is crucial

---

[1]The light yield is defined as 1 for electron recoils of $122\,\mathrm{keV}$, i.e. the light energy of such events is defined as $122\,\mathrm{keV_{ee}}$, the so-called electron-equivalent energy [15].

for the requirements in terms of radiopurity. Since radioactive isotopes in CaWO$_4$ crystals can originate from the raw materials themselves [20], a careful selection of these materials is necessary. In particular, in CaCO$_3$ powders which are often extracted from geological settings considerable contaminations were found (e.g. ^{226}Ra with an activity of $\mathcal{O}(10\,\text{mBq/kg})$ [20]). Beyond that, impurities can be introduced during processing and handling of raw materials, during crystal growth and detector production. An important source of contamination is Rn-implantation from air. The gaseous isotope ^{222}Rn (half-life 3.6 d) which is produced in the U-238 chain easily escapes from solid material, whereas its solid daughter nuclei stick to surfaces. Therefore, in particular the surfaces of the detectors and of their surroundings get contaminated and the exposure to air containing Rn has to be minimized. Further, storing CaWO4, which is often delivered as a powder, requires adequate storage to minimize Rn-related backgrounds.

3   Experimental results

The first data of TUM40 in CRESST-II Phase 2 with an exposure of 29 kg-days were used for a low-mass WIMP analysis [8] and for the background studies presented in this paper.

3.1   Beta/gamma background

The dominant part of events observed with CRESST-II detector modules are gamma or beta induced electron recoils which result in a highly populated beta/gamma band. At lowest energies ($E \lesssim 10\,\text{keV}$), due to the finite resolution of the light detector there is a strong overlap with the ROI for dark matter search. Therefore, the beta/gamma background level is crucial for the sensitivity of CRESST-II detectors.

The low-energy spectra ($E \leq 100\,\text{keV}$) of commercially available CaWO$_4$ crystals are usually dominated by two intrinsic beta/gamma background components [21]:

- Beta-decays of ^{210}Pb which is part of the U-238 chain. It decays into ^{210}Bi with a half-life of 22.3 years [22]. In 84% to all cases, an excited energy state of ^{210}Bi with an energy of 46.5 keV is populated. If the contamination is intrinsic to the crystal, both, the energy of the de-excitation gamma and that of the corresponding electron are detected in the crystal. These energy depositions cannot be resolved as separate events with cryogenic detectors and, hence, the two signals add. In many crystals, prominent ^{210}Pb beta spectra are visible (decreasing in intensity from 46.5 keV towards the Q-value of 63.5 keV) which are evidence of a strong internal contamination. If a ^{210}Pb decay takes place on surfaces of materials outside the detector modules, only the de-excitation gamma is detected which results in a distinctive peak at 46.5 keV (external contamination).

- Beta-decays of ^{227}Ac which is part of the U-235 chain. It decays to ^{227}Th with a half-life of 21.8 years [22]. In 35% (10%) of the decays, an excited state of the daughter nucleus at the energy level of 24.5 keV (9.1 keV) is populated which relaxes by gamma-emission to the ground state. Therefore, 3 beta-spectra are visible, each of them extending up to the Q-value of 44.8 keV with two characteristic edges at 24.5 keV and 9.1 keV [23].

In figure 2, the characteristic features of ^{210}Pb and ^{227}Ac are clearly visible in the spectrum (black dashed line) of the crystal "VK31" which is operated in CRESST-II Phase 2. The mean background rate in the ROI is about 30 counts/[kg keV day] which is a typical value

for CaWO$_4$ crystals of that supplier.[2] The best such commercial crystal in terms of intrinsic radiopurity, called "Daisy", has an average rate of ~ 6 counts/[kg keV day] (red dashed line in figure 2).

For the first time, a detailed beta/gamma-background study of a TUM-grown crystal (TUM40) was performed in this paper. The bulk contamination and the average background rate could significantly be reduced to 3.51/[kg keV day] in the ROI which is a reduction by a factor of 2-10 compared to commercial CaWO$_4$ crystals. The histogram in figure 2 shows the low-energy spectrum of TUM40 from the first 29 kg-days exposure of CRESST-II Phase 2. Distinct gamma peaks appear above a rather flat background which was not observed with commercial crystals. The dominant ones could be identified to originate from cosmogenic activation of W isotopes:

- Proton capture on ^{182}W (and a successive decay) can result in ^{179}Ta which decays via EC to ^{179}Hf with a half-life of 665 d. The EC signature in our detectors is exactly the binding energy of the shell electrons of ^{179}Hf. In addition to a peak at 65.35 keV (K-shell) which was reported earlier [21] also distinct peaks at 11.27 keV (L1-shell), 10.74 keV (L2-shell) and 2.60 keV (M1-shell) could be identified here. The energies of all identified lines agree within errors with literature values and are listed in table 1 with their corresponding activities. For the latter, the detection efficiency of TUM40 is considered (see [8]). The K-shell EC line of ^{179}Ta has the highest rate: $A_K = (277.2 \pm 15.7)\,\mu$Bq/kg.

- Proton capture on ^{183}W can result in ^{181}W which decays via electron capture (EC) to ^{181}Ta with a half-life of 121 d. We confirm the presence of a line at 74.02 keV (K-shell + 6.2 keV gamma) [21] with an activity of $A_K = (58.1 \pm 14.5)\,\mu$Bq/kg. To observe higher-order shell EC processes, present statistics is not yet sufficient.[3]

In addition, gamma lines from external radiation can be identified: lines at 46.54 keV from ^{210}Pb and, at higher energies, from ^{234}Th, ^{226}Ra, ^{212}Pb, ^{208}Tl, ^{214}Bi, ^{228}Ac and ^{40}K. A peak from copper X-ray fluorescence at 8.05 keV (K$_\alpha$) is observed since most of the material surrounding the detector is copper. The corresponding activities are listed in table 1. The contribution of these lines to the background in the ROI is investigated in section 4.

There are no obvious features of beta spectra visible in the data of TUM40. However, the background contribution of beta/gamma decays from natural decay chains could be derived by a detailed analysis of the alpha spectra (see section 3.3) in combination with a dedicated MC simulation (see section 4).

3.2 Surface-alpha background

A very detailed description of the crucial backgrounds related to surface alpha-events is given in [15]. Here, the basic results of that analysis are presented.

The data of CRESST-II detectors is often displayed in the light yield vs. energy plane, as shown in figure 3 for TUM40: at light yields of ~ 1 the dominant beta/gamma band arises, almost horizontal at energies $\gtrsim 50$ keV and slightly decreasing (in light yield) towards smaller energies due to the scintillation properties of CaWO$_4$ [23]. The parametrisation of

---

[2]The crystals were supplied by the General Physics Institute of the Russian Academy of Sciences (Moscow, Russia).

[3]Since CRESST-II Phase 2 is planned to run for ~ 2 years a further confirmation of these peaks is in reach by comparing the evolution of the event rate over time with the expected half-lifes.
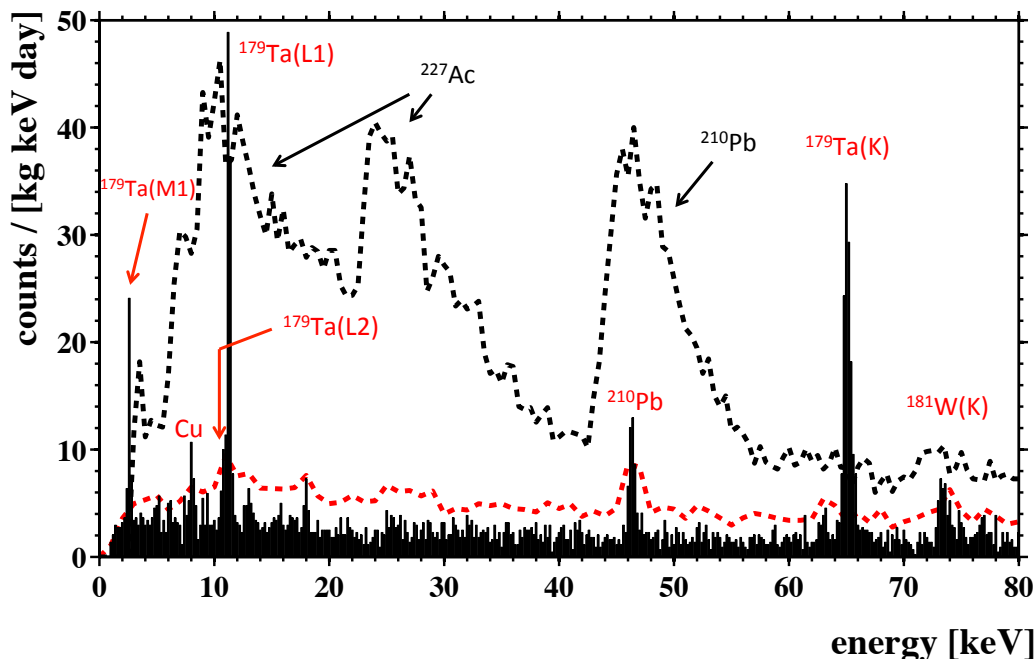
Figure 2. Histogram of the low-energy events (black bars) recorded during CRESST-II Phase 2 with TUM40 which was produced at the Technische Universität München. The most prominent peaks are labelled (in red). In comparison, the background levels of commercial $CaWO_4$ crystals operated as detectors in CRESST II Phase 2 are shown. The dashed red line indicates the rate of the crystal "Daisy" which has the lowest background rate among all commercial crystals (~ 6 counts/[kg keV day]). The dashed black line shows the background of a typical commercial crystal, called "VK31" (~ 30 counts/[kg keV day]). In that, the characteristic beta spectra of ^{227}Ac and ^{210}Pb clearly dominate.

the event bands is given in [15]. The ROI for dark matter search, including all 3 nuclear recoil bands from threshold to 40 keV,[4] is shown as a grey area in figure 3. The reference region for ^{206}Pb recoils induced by ^{210}Po alpha decays is also indicated in the plot (area enclosed by the green line) at light yields of ~ 0.01 between 40 keV and 107 keV. In earlier runs of CRESST-II this region was populated: at the full kinetic energy of the Pb nucleus (decay on surfaces of surrounding material and of the crystal) a peak arose at ~ 103 keV with a exponential tail towards lower energies. The latter comes from ^{210}Po decays which are implanted in surrounding material. It was identified to originate from a contamination in the metal clamps holding the crystals (e.g. by Rn-implantation from air). The resulting spectrum of Pb-recoils was reproduced by a SRIM simulation [18].

In the first data of TUM40 acquired in CRESST-II Phase 2 no events are observed in the reference region for ^{206}Pb recoils, while with the background level of Phase 1 [18] 6.9 ± 2.6 events would be expected. Since in the novel detector module (see section 2) the crystal is completely surrounded by scintillating materials, the corresponding alpha with an energy of ~ 5.3 MeV produces sufficient additional light to shift ^{206}Pb recoils out of the nuclear recoil region. A population of such vetoed events is visible in figure 3 at light yields of 0.2-0.5 (red dots). This first data show the high efficiency of the surface-alpha event rejection realized

---

[4]In [8], the 50% acceptance bound for O recoils is defined as the upper light yield bound for the ROI. This convention is also used in this paper.

source	E_{lit} [keV] [22]	$A\,[\mu\mathrm{Bq/kg}]$
^{179}Ta (M1)	2.6009	70.3±15.8
Cu X-ray (ext.)	8.048	27.1 ±14.3
^{179}Ta (L2)	10.74	24.8±14.5
^{179}Ta (L1)	11.271	202.2±16.0
^{210}Pb (ext.)	46.54	78.6±14.8
^{179}Ta (K)	65.35	277.2±15.7
^{181}W (K)	74.02	58.1±14.5
^{234}Th (ext.)	92.4	123.5±11.7
^{226}Ra (ext.)	186.2	109.0±11.2
^{212}Pb (ext.)	238.6	185.6±12.9
^{208}Tl (ext.)	583.2	93.4±8.4
^{214}Bi (ext.)	609.2	69.3±24.6
^{228}Ac (ext.)	911.2	54.8±6.8
^{228}Ac (ext.)	969.0	36.3±6.1
^{40}K (ext.)	1432.7	41.4±6.2
^{208}Tl (ext.)	2614.0	28.5±3.9

Table 1. Activities A of the identified gamma-lines measured with the crystal TUM40 in 29 kg-days of exposure during CRESST-II Phase 2. External gamma lines (ext.) as well as peaks from cosmogenically-induced EC decays are listed (the shell of the captured electron is shown in brackets).

with the new detector concept. No such backgrounds are expected within the sensitivity goals of CRESST-II Phase 2 with the final exposure [15].

Furthermore, an additional background source most probably originating from contaminations on surfaces of materials outside the detector housing was identified in this paper. Electrons (e.g. from beta-emitters from natural decay chains) pass through the polymeric foil (thickness 50 μm), lose some of there energy therein and produce additional light before getting absorbed by the CaWO$_4$ crystal. Dedicated measurements show that electrons, independent of there energy, produce a roughly fixed amount of scintillation light in the foil with an energy of $\mathcal{O}(1\,\mathrm{keV})$. This explains the additional population of events above the beta/gamma band (labelled by "external betas" in figure 3). Since an approximately fixed amount of addition scintillation light adds to the light produced by the beta in the crystal, the excess in light yield gets bigger towards lower energies. The analysis performed in section 4 finds a significant contribution of this event population to the overall background in the ROI.

3.3 Alpha background

Due to the phonon-light technique of CRESST-II detectors, alpha events can be perfectly discriminated from other backgrounds, particularly, from the dominant beta/gamma populations. In case of an internal contamination, the full energy (Q-value) of a decay is measured. Therefore, the most obvious approach to investigate intrinsic radioactivity of CaWO$_4$ crystals is the analysis of discrete alpha lines which arise at energies $\gtrsim 2\,\mathrm{MeV}$ far off the ROI.
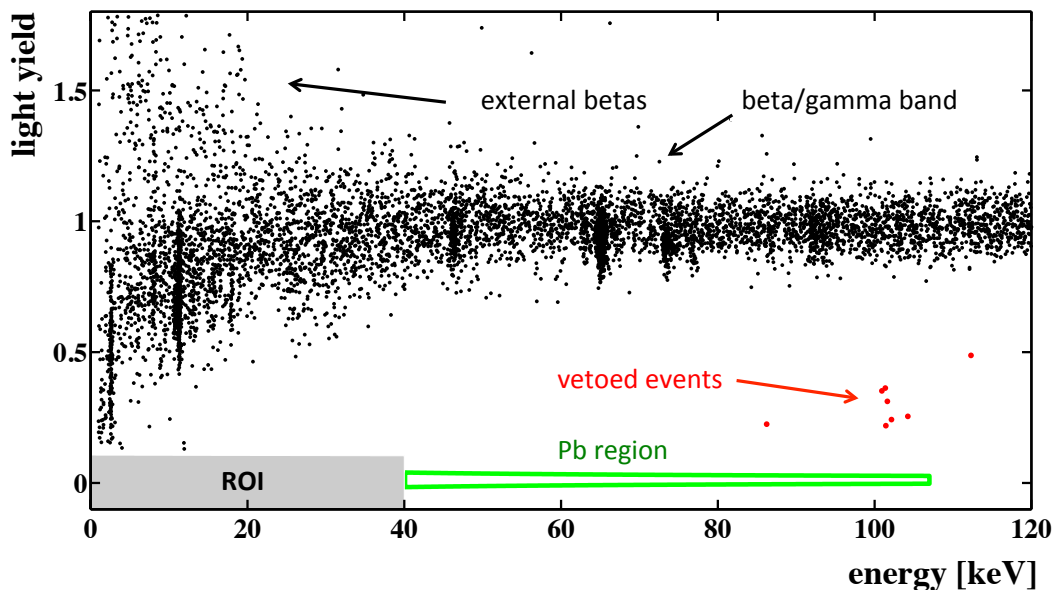
Figure 3. Light yield vs. energy plot of the events (dots) recorded with TUM40 in CRESST-II Phase 2. At light yields of ~ 1 the dominant band of beta/gamma events shows up. Due to light quenching [16] nuclear recoils have a reduced light yield. The ROI for dark matter search is shown in grey. Surface-alpha related ^{206}Pb recoil background would be expected in the region enclosed by the green line. Due to the scintillation veto of the novel detector module, this area is free of events. All ^{206}Pb recoils observed are shifted to higher light yields (red dots). External betas passing through the scintillating foil show up at higher light yields compared that of events in the beta/gamma band.

Distinct alpha peaks from intrinsic contamination of the natural decay chains as well as of radioactive rare-earth metals (e.g. ^{147}Sm) and the isotope ^{180}W are observed.

With TUM40 decays from the three natural decay chains U-238, U-235 and Th-232 are observed. All individual decays are listed with their respective half-life and Q-values (E_{lit}) in table 2. The detailed study of the intrinsic alpha contaminations performed in this work, enables to derive all relevant beta-decay rates. This provides a quantification of the intrinsic contamination at low-energies for the first time.

The large dynamic range and the discrimination capability of CRESST-II detectors for alpha events is illustrated in figure 4. The energy measured in the phonon detector is plotted versus the (electron-equivalent) energy measured in the light detector with the module TUM40 in 29 kg-days of exposure. Due to light quenching the alpha band is well-separated from the beta/gamma band. Besides lines from ^{147}Sm and ^{180}W, all peaks can be attributed to alpha decays from natural decay chains clustering at energies between 4 and 7 MeV. The total alpha activity from intrinsic contamination is $A_{\mathrm{tot}} = (3.08 \pm 0.04)$ mBq/kg to which ^{238}U $((1.01 \pm 0.02)$ mBq/kg) and ^{234}U $((1.08 \pm 0.03)$ mBq/kg) from the U-238 chain are the dominant contribution. The histogram in figure 5 shows the identified alpha peaks of lower intensities $((\sim 10 - 100)\,\mu$Bq/kg) between 4 and 7 MeV. At even higher energies beta-alpha coincident events are visible in figure 4 (^{214}Bi/^{214}Po and ^{212}Bi/^{212}Po at $\sim 7.8 - 12$ MeV). These subsequent decays are too fast to be disentangled as separate events by CRESST-II detectors, hence both signals sum up and characteristic continuous bands arise (see [20] for details). Similarly, the alpha-alpha coincidence ^{219}Rn/^{215}Po shows up at the combined energy

chain	parent	mode	br [%]	half-life	E_{lit} [keV]	E_{obs} [keV]	$A\,[\mu\mathrm{Bq/kg}]$
^{238}U	^{238}U	α	100	$4.47 \cdot 10^9$ y	4270	4271	$(1.01\pm0.02)\cdot10^3$
	^{234}Th	β^-	100	24.1 d	273	0-273	(a)
	^{234}Pa*	β^-	100	1.17 min	2197	0-2197	(a)
	^{234}U	α	100	$2.45 \cdot 10^5$ y	4858	4853	$(1.08\pm0.03)\cdot10^3$
	^{230}Th	α	100	75.4 y	4770	4771	55.8±5.4
	^{226}Ra	α	100	1.60 y	4871	4853 (b)	43.0±9.9
	^{222}Rn	α	100	3.82 d	5590	5592	38.1±4.9
	^{218}Po	α	99.98	3.10 min	6115	6139	43.1±9.9
	^{214}Pb	β^-	100	26.8 min	1023	0-1023	(a)
	^{214}Bi	β^-	99.98	19.9 min	3272	7800-11000	47.4±4.9
	^{214}Po	α	100	0.164 ms (c)	7883		
	^{210}Pb	β^-	100	22.3 y	63.5	0-63.5	7^{+36}_{-7}
	^{210}Bi	β^-	100	5.01 d	1163	0-1163	(a)
	^{210}Po	α	100	138 d	5407	5403	17.8±4.0
^{235}U	^{235}U	α	100	$7.04 \cdot 10^8$ y	4678	4671	39.5±4.4
	^{231}Th	β^-	100	25.52 h	389.5	0-389.5	(a)
	^{231}Pa	α	100	$3.27 \cdot 10^4$ y	5150	5139	23.2±4.4
	^{227}Ac	β^-	98.62	21.8 y	44.8	0-44.8	98±20
	^{227}Th	α	100	18.7 d	6147	6139	105±19
	^{223}Ra	α	100	11.4 d	5979	5968	104±7
	^{219}Rn	α	100	3.96 s	6946	14900	107±7
	^{215}Po	α	100	1.78 ms (c)	7527		
	^{211}Pb	β^-	100	36.1 min	1373	0-1373	(a)
	^{211}Bi	α	100	0.51 s	6751	6771	105±7
	^{207}Tl	β^-	100	4.77 min	1423	0-1423	(a)
^{232}Th	^{232}Th	α	100	$1.40 \cdot 10^{10}$ y	4083	4084	9.2±2.3
	^{228}Ra	β^-	100	5.75 y	45.9	6.7-45.9	(a)
	^{228}Ac	β^-	100	6.15 h	2127	58-2127	(a)
	^{228}Th	α	100	1.91 y	5520	5518	15.2±4.1
	^{224}Ra	α	100	3.63 d	5789	5788	19.8±8.1
	^{220}Rn	α	100	55.6 s	6404	6414	8.4±3.4
	^{216}Po	α	100	0.145 s	6906	-	0
	^{212}Pb	β^-	100	10.64 h	573.7	0-573.7	(a)
	^{212}Bi	α	35.94	60.6 min	6208	6216	$7.7^{+8.9}_{-7.7}$
		β^-	64.06		2252	8900-11200	15.8±2.8
	^{212}Po	α	100	299 ns (c)	8955		
	^{208}Tl	β^-	100	3.01 min	5001	3197-5001	(a)

Table 2. Radioactive decays (alpha and beta) of the natural decay chains (U-238, U-235 and Th-232) from intrinsic contamination observed with the crystal TUM40. The first 29 kg-days of exposure of CRESST-II Phase 2 were used for the analysis. The Q-values (E_{lit}) from literature [22] of the individual reactions are compared with the energies (E_{obs}) observed in the detector. The corresponding activities A are given with 1σ errors. The branching ratios (br) of the individual reactions are listed. The symbol (a) indicates beta decays which cannot be identified individually but are in equilibrium with short-lived alpha decays. Alpha-lines marked with (b) have a significant overlap with stronger alpha sources. The symbol (c) indicates fast decays which cannot (or only partly) be distinguished from the proceeding decay within detector resolution. The total activity of the identified intrinsic alpha sources is $A_{tot,\alpha} = 3.08\pm0.04\,\mathrm{mBq/kg}$.
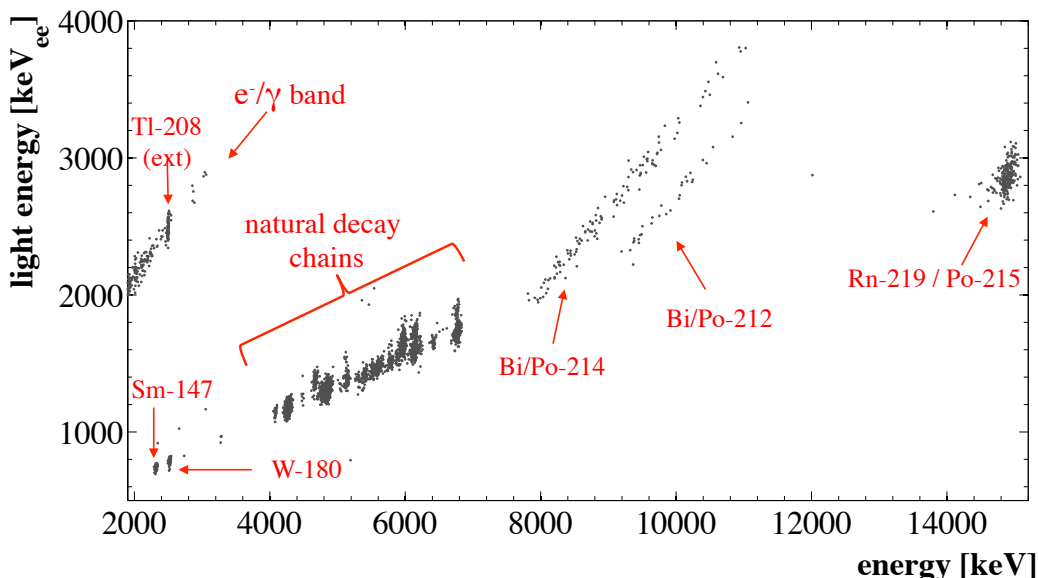
Figure 4. Energy measured in the phonon detector plotted against the energy detected in the light detector in units of electron-equivalent energy (keV$_{ee}$). The alpha lines are well separated from the beta/gamma band due to light quenching ($QF_\alpha \sim 0.22$). Most of the discrete alpha lines of the natural decay chains have energies between 4 and 7 MeV (see figure 5) except the $\alpha-\alpha$ (^{219}Rn/^{215}Po) and $\alpha-\beta$ (^{214}Bi/^{214}Po, ^{212}Bi/^{212}Po) coincidences at higher energies. Lines from intrinsic ^{180}W and a contamination of ^{147}Sm are also visible.

of ~ 14.9 MeV. The measured ^{180}W activity of $(36 \pm 9)\,\mu$Bq/kg agrees well with the rate of $(31 \pm 8)\,\mu$Bq/kg obtained by a previous measurement [24] which cross-checks the analysis performed.

All alpha particles from natural decay chains are observed in this data and the corresponding activities are listed in table 2. All alpha decays, short-lived with respect to the measuring time (~ 0.5 y) agree in rate as expected. The equilibrium of the U-238 chain is broken at the long-lived isotopes ^{234}U[5] and that of the U-235 chain at ^{231}Pa. This can originate, e.g., from chemical separation processes during the production steps. All measured intensities are consistent with the individual decay chains (a reduced detection efficiency for the decays ^{220}Rn and ^{216}Po due to pile-up effects has to be considered, for details see [20]).

4   Monte Carlo based decomposition of the background

By the detailed alpha analysis presented in section 3.3 the intensities of all beta decays from the natural decay chains U-238, U-235 and Th-232 can be derived since they are in equilibrium with at least one alpha decay (see table 2). These measured activities were used as input for a dedicated GEANT4 MC simulation (version 10.1) [25, 26] which allows to derive the beta/gamma spectra in the ROI for dark matter search. To model the production, propagation, and absorption of beta/gamma particles in the detector down to 250eV, the Livermore low-energy electromagnetic models were used. The electromagnetic model im-

---

[5]A broken equilibrium at ^{210}Pb and ^{210}Po (U-238 chain) is possible, however, can not be proven here due to limited statistics.
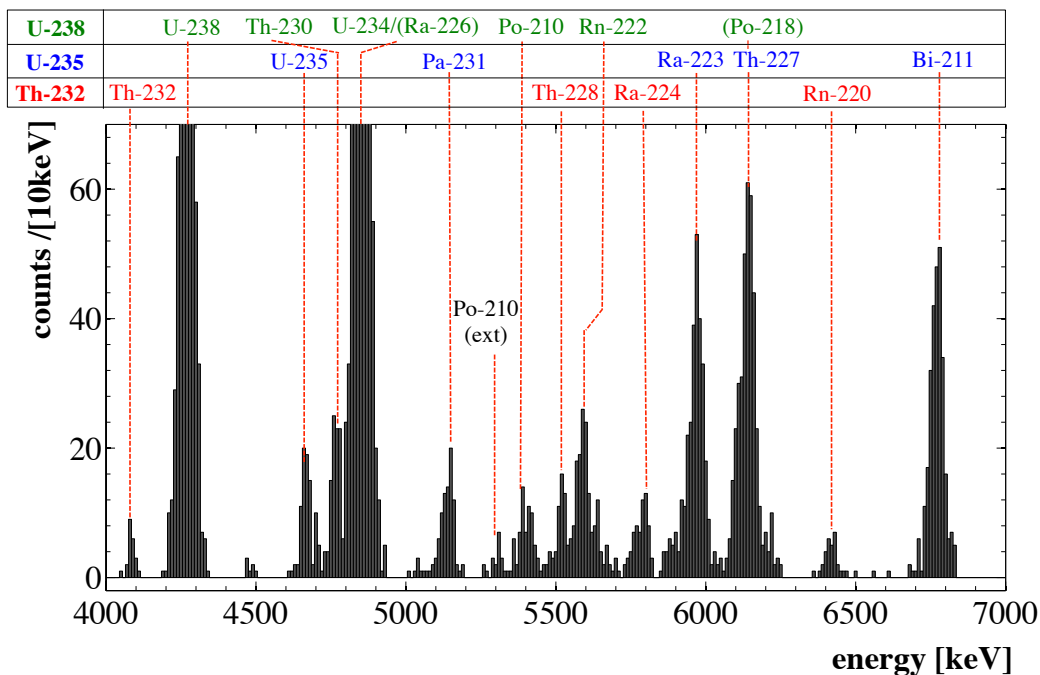
Figure 5. Discrete alpha lines from the natural decay chains observed with the crystal TUM40 in an exposure of 29 kg-days between 4 and 7 MeV. The lines identified in the U-238, U-235 and Th-232 chains are listed. In addition, an external ^{210}Po line is visible where only the alpha energy (5.30 MeV) and not the recoil of ^{206}Pb (103 keV) is detected. The individual activities are listed in table 2. The peaks of ^{238}U and ^{234}U completely dominate the spectrum (upper cut in histogram at 70 counts/[10 keV]).

plements photo-electric effect, Compton scattering, Rayleigh scattering, conversion in e⁺e⁻ pairs, ionisation, and bremsstrahlung production.

The results of this data-based simulation is shown in figure 6 (inset): the blue curve shows the sum of all beta/gamma events from natural decay chains. The 1-σ error band (light blue) is a combination of the statistical error of the simulation and the uncertainty of the experimentally determined activities of the beta emitters. This contribution has an activity of $A_{1-40} = 494.2 \pm 48.4\,\mu$Bq/kg in the ROI which corresponds to a mean rate of 3.51 ± 0.09 counts/[kg keV day]. For the first time, the contribution of the intrinsic beta/gamma emitter could be disentangled and accounts for $(30.4 \pm 2.9)\%$ of the total events observed. The main contributions originate from ^{234}Th ($346\,\mu$Bq/kg), ^{227}Ac ($93\,\mu$Bq/kg), ^{234}Pa ($35\,\mu$Bq/kg) and ^{228}Ra decays ($9\,\mu$Bq/kg). The characteristic edges at ~ 9 keV and ~ 24 keV originate from the contribution of the ^{227}Ac spectrum (see section 3.1). The values of all relevant beta emitters are listed in table 3.

Furthermore, the response of the detector to external gamma radiation is studied with a dedicated MC simulation. The intensity of the individual components is scaled such to match the observed external gamma peaks (see section 3.1). All identified external gamma lines which are listed in table 1 are included in the study. The result is shown as in figure 6 (inset) as a green line with the corresponding 1-σ error band (light green). The only peak in the ROI identified as to originate from external radiation is the Cu X-ray peak at 8.0 keV. The continuous Compton background from external sources (peaks at higher energies) is

negligible in the ROI ($\lesssim$ 0.03 events/[kg keV day]), however, W-escape peaks originating from the ^{234}Th line at around 92.4 keV contribute significantly ((62.2 ± 7.8) μBq/kg). X-rays from W (K$_{\alpha 1}$: 59.3 keV, K$_{\alpha 2}$: 58.0 keV, K$_{\beta 1}$: 67.2 keV and K$_{\beta 2}$: 69.1 keV [22]) can escape the CaWO$_4$ crystal giving rise to 4 distinct escape peaks between 23 and 35 keV. The statistics of the recorded data is not yet sufficient to resolve these peaks, but as shown below, the total observed spectrum is compatible with this prediction.

In addition to that, a background component from external betas has been identified within this work. As explained in section 3.2, electron passing through the polymeric foil produce additional scintillation light before hitting the CaWO$_4$ crystal which shifts these events to higher light yields (see figure 3). A phenomenological model to account for this event population was developed in [27]. Measurements show that these events can be nicely described by an exponential distribution decreasing towards higher energies and higher light yields. To obtain the observed event distribution, the spectrum has to be convolved with the resolution of the light measurement. A detailed description of the likelihood fit performed can be found in the literature [15, 27]. The result of the likelihood fit to the data of TUM40 is shown in figure 6 (inset): the grey curve accounts for the rate of external betas most probably originating from beta emitters on surfaces surrounding the detectors. The corresponding 1-σ error bounds are depicted in light grey. An activity of (274 ± 137.6) μBq/kg which corresponds to (16.9 ± 8.4)% of the total rate is attributed to external betas.

The EC-peaks (at 2.60 keV, 10.74 keV and 11.27 keV) originating from cosmogenic activation of W isotopes (see section 3.1) account for (290.7 ± 17.0) μBq/kg ((17.9 ± 1.0)% of the total rate).

The red curve in figure 6 (main frame and inset) shows the combined spectrum of all identified backgrounds. The inset shows the corresponding 1-σ error bounds (light red). A total activity of (1121.8 ± 146.6) μBq/kg is found which explains (69.0 ± 9.0)% of the data. While at energies above ~ 20 keV the sum of identified sources almost completely reproduces the data, at lower energies a significant part of the spectrum remains unexplained. There are slight hints for additional gamma peaks (e.g at ~ 18 keV), for the identification of which, however, more statistics is necessary.

To investigate the relevance of the individual background components for dark matter search, their leakage into the nuclear-recoil bands is calculated based on the background studies developed in this work. The number of events leaking into the ROI (to below the 50% acceptance bound for O-recoils [8]) is calculated for the beta/gamma spectrum from natural decay chains, external gammas, the cosmogenic activation lines and the contribution of external betas. In table 3 the cumulative leakage of the individual components into the ROI is listed for an analysis threshold of 1 keV (L_1) and 12 keV (L_{12}). The cumulative leakage is graphically illustrated in figure 7 as a function of the analysis threshold. For an analysis threshold of 1 keV a leakage of $\mathcal{O}(10^2)$ events per detector and year is expected. Here the contaminations due to cosmogenic activation give the highest contribution. Above ~ 12 keV, the leakage drops by ~ 2 orders of magnitude and is then dominated by intrinsic beta/gamma events. The calculation shows that an experiment would be background-free up to an exposure of ~ 3 ton-years.
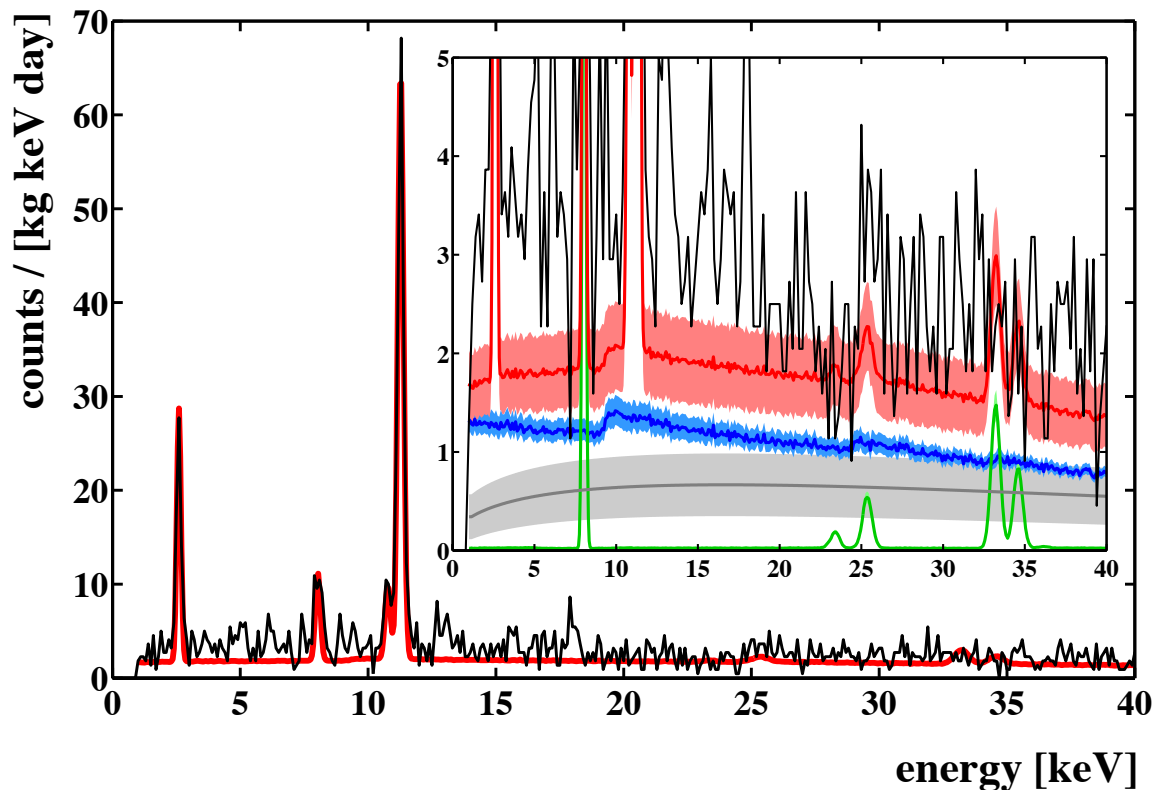
Figure 6. Histogram of the events in the ROI (black line) recorded with TUM40 in CRESST-II Phase 2. The red line indicates the sum of all identified background sources with the dominant peaks from cosmogenic activation (2.6 keV, 10.7 keV, 11.3 keV) and the Cu X-ray line (8.0 keV). Inset: decomposition of the background based on MC simulation (see text). The contributions of external gamma radiation (green), external betas (grey) and intrinsic beta/gamma radiation from natural decay chains (blue) are shown. The sum of these components (plus gamma peaks) are shown in red. The individual 1-σ error bands are depicted in the corresponding colour. The identified backgrounds explain $\sim$70% of the observed events.

5 Conclusions and outlook

TUM40 operated in the new detector housing has reached unprecedented background levels. Using CaWO$_4$ sticks to hold the target crystal, a fully-scintillating inner detector housing is realized and backgrounds from surface-alpha decays are rejected with high efficiency. A phonon trigger threshold of $\sim$ 0.60 keV and a resolution of σ=(0.090±0.010) keV (at 2.60 keV) are reached with TUM40. By using a CaWO$_4$ crystal produced at the TUM, the intrinsic background rate was reduced to the lowest level reported for CRESST CaWO$_4$ detectors: on average 3.51 ± 0.09 beta/gamma events per kg keV day in the ROI (1-40 keV) and a total alpha activity from natural decay chains of $A_{tot,\alpha} = 3.08 \pm 0.04$ mBq/kg. In this paper, a detailed alpha analysis was performed which allowed to derive the activities of all decaying isotopes of the natural decay chains. Based on these results, a GEANT4 MC simulation was set up to investigate the contribution of intrinsic beta/gamma backgrounds in the ROI for dark matter search (1-40 keV). An activity of $\sim$ 494 μBq/kg was found which corresponds to $\sim$ 30% of the total event rate. The MC simulation also shows the contribution of events originating from external gamma radiation. An activity of 62.2 μBq/kg ($\sim$ 4% of total) is

source	A_{1-40} [μBq/kg]	L_1/[det.-y]	L_{12}/[det.-y]
^{234}Th	346.2 ± 12.3	18.1	$2.0 \cdot 10^{-5}$
^{234}Pa*	35.0 ± 5.7	1.6	$2 \cdot 10^{-6}$
^{214}Pb	$(8.3 \pm 0.4) \cdot 10^{-1}$	$3.7 \cdot 10^{-2}$	$< 10^{-6}$
^{210}Pb	1.0 ± 0.1	$8.6 \cdot 10^{-2}$	$< 10^{-6}$
^{210}Bi	$(3.6 \pm 0.4) \cdot 10^{-1}$	$1.6 \cdot 10^{-2}$	$< 10^{-6}$
^{231}Th	$1.1 \cdot 10^{-2}$	$2.5 \cdot 10^{-4}$	$< 10^{-6}$
^{227}Ac	92.9 ± 1.8	5.6	$9.0 \cdot 10^{-6}$
^{211}Pb	4.2 ± 0.1	$1.9 \cdot 10^{-1}$	$< 10^{-6}$
^{207}Tl	3.9 ± 0.6	$1.7 \cdot 10^{-1}$	$< 10^{-6}$
^{228}Ra	8.9 ± 0.2	$8.3 \cdot 10^{-4}$	$1 \cdot 10^{-6}$
^{212}Pb	$(2.4 \pm 0.4) \cdot 10^{-1}$	$1.1 \cdot 10^{-2}$	$< 10^{-6}$
Cu X-ray (ext.)	27.1 ± 5.1	$4.4 \cdot 10^{-4}$	-
Σ internal β/γ	494.2 ± 48.4	25.7	$3.2 \cdot 10^{-5}$
Σ cosmogenics	290.7 ± 17.0	40.8	$< 10^{-6}$
Σ external γ	62.2 ± 7.8	$3.9 \cdot 10^{-1}$	$1 \cdot 10^{-6}$
Σ external β	274.7 ± 137.6	7.8	$1.6 \cdot 10^{-5}$
Σ all identified	1121.8 ± 146.6	74.7	$4.9 \cdot 10^{-5}$
total observed	1625.1 ± 40.3	108.3 (a)	$7.1 \cdot 10^{-5}$ (a)

Table 3. Activities (A_{1-40}) of the identified background sources in the e^-/γ-band between 1 and 40 keV and the expected leakage L_1 (L_{12}) per detector ($m = 245$ g) and year into the region-of-interest (ROI) assuming an analysis threshold of 1 keV (12 keV). The activities of the relevant β^--decaying isotopes from natural decay chains are derived by a MC-based analysis (see text). The sum of all intrinsic beta decays (Σ internal β/γ), of the cosmogenic activation lines (Σ cosmogenics), of the external γ radiation (Σ external γ) and of the external β radiation (Σ external β) are listed. The sum of all identified sources is compared to the activity observed with in the data of CRESST-II Phase 2. For L_1 and L_{12} the total errors are of $\mathcal{O}(10\%)$. (a) indicates an extrapolation to the assumed exposure of 1 detector-year.

found in the ROI. Furthermore, the study shows that 17% of the background most probably is due to electrons originating from surfaces surrounding the detector and passing through the scintillating housing. Distinct gamma lines are observed in the low-energy spectrum at energies < 80 keV, originating from cosmogenic activation of W isotopes. The isotopes ^{182}W and ^{183}W, and subsequent EC-reactions of ^{179}Ta and ^{181}W are identified as sources. The resulting activity in the ROI is 290.7 μBq/kg ($\sim 18\%$ of the total event rate).

For the first time, the background in the ROI of a CRESST-II detector module could be decomposed in a comprehensive way. The analysis performed suggests that the background of TUM40 is - unlike previously assumed - not exclusively limited by intrinsic contaminations from natural decay chains, but cosmogenic activation and external sources play an important role. The knowledge of the background origin is crucial for the future R&D activities of CRESST concerning background reduction.

The sensitivity of CRESST-II detectors for dark matter search was investigated by calculating the leakage of beta/gamma events into the ROI. For analysis thresholds > 12 keV
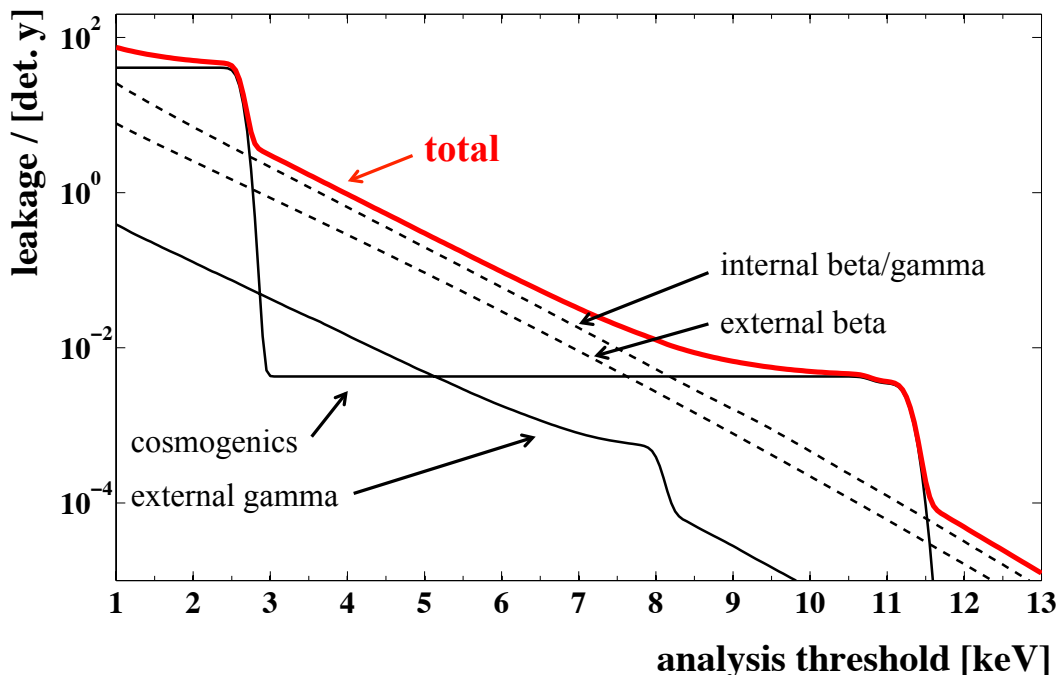
Figure 7. Expected cumulative leakage from the beta/gamma band into the ROI (1 to 40keV) plotted against the analysis threshold. The calculation is based on the background level of the detector TUM40 in CRESST-II Phase 2. The decomposition of the background into individual components is explained in detail in section 4.

the present background level results in a total expected leakage of $< 10^{-4}$ events per detector and year. This suggests that even for a ton-scale experiment and typical measuring times of $\mathcal{O}(1\,\mathrm{year})$ such detectors would not be limited by beta/gamma leakage and, if no additional background sources contribute, would be background-free for high WIMP-mass searches ($\gtrsim 5\,\mathrm{GeV}/c^2$). The goals of the future EURECA experiment [28], namely to reach the level of 10^{-10} pb for the spin-independent WIMP-nucleon scattering cross-section (for WIMP masses of $\sim 50\,\mathrm{GeV}/c^2$), can be achieved by TUM40-type detectors using state-of-the-art CRESST technology.

Due to the low thresholds achieved, CRESST detector are most suited for the detection of low-mass WIMPs ($\lesssim 5\,\mathrm{GeV}/c^2$). The potential has been recently demonstrated by the first data of TUM40 in CRESST-II Phase 2 which sets stringent limits on the WIMP-nucleon scattering cross-section and explores new parameter space below WIMP masses of $3\,\mathrm{GeV}/c^2$ [8]. The study performed in this paper shows that for an analysis threshold of $1\,\mathrm{keV}$ a total leakage of $\sim 10^2$ events is expected per detector and year. This agrees nicely with the number of events observed in the ROI during the first 29 kg-days of data acquired with TUM40 and suggests that no other background sources contribute (as e.g. neutrons). To achieve the future sensitivity goals for low-mass WIMP search [29], background levels must be further reduced. External radiation can be diminished by cleaning of material which are in the vicinity of the detectors (e.g. re-etching of copper surfaces) and additional shielding. To reduce the crystal-intrinsic backgrounds, the crystal production at TUM is key. We plan to significantly reduce the cosmogenic activation of W isotopes by using only screened and assayed materials, and to shorten the exposition to cosmic rays during transport and

storage. It was found, that the growth procedure itself segregates certain radioactive isotopes significantly. Comparing the contamination of ^{226}Ra in TUM40 ((43.0 ± 9.9) μBq/kg, see table 2) with that in the raw materials ($\mathcal{O}(10\,\text{mBq/kg})$ [20]), a purification by almost 3 orders of magnitude is achieved. Therefore, a multiple re-crystallization of $CaWO_4$ crystals is a promising technique to decrease both, cosmogenic activation and contaminations from natural decay chains.

Acknowledgments

References

[1] G. Bertone, D. Hooper and J. Silk, *Particle dark matter: Evidence, candidates and constraints*, *Phys. Rept.* **405** (2005) 279 [hep-ph/0404175] [INSPIRE].

[2] G. Jungman, M. Kamionkowski and K. Griest, *Supersymmetric dark matter*, *Phys. Rept.* **267** (1996) 195 [hep-ph/9506380] [INSPIRE].

[3] LUX collaboration, D.S. Akerib et al., *First results from the LUX dark matter experiment at the Sanford Underground Research Facility*, *Phys. Rev. Lett.* **112** (2014) 091303 [arXiv:1310.8214] [INSPIRE].

[4] P. Cushman et al., *Working Group Report: WIMP Dark Matter Direct Detection*, arXiv:1310.8327 [INSPIRE].

[5] DAMA and LIBRA collaboration, R. Bernabei et al., *New results from DAMA/LIBRA*, *Eur. Phys. J.* **C 67** (2010) 39 [arXiv:1002.1028] [INSPIRE].

[6] CoGeNT collaboration, C.E. Aalseth et al., *CoGeNT: A search for Low-Mass Dark Matter using p-type Point Contact Germanium Detectors*, *Phys. Rev.* **D 88** (2013) 012002 [arXiv:1208.5737] [INSPIRE].

[7] CDMS collaboration, R. Agnese et al., *Silicon Detector Dark Matter Results from the Final Exposure of CDMS II*, *Phys. Rev. Lett.* **111** (2013) 251301 [arXiv:1304.4279] [INSPIRE].

[8] CRESST-II collaboration, G. Angloher et al., *Results on low mass WIMPs using an upgraded CRESST-II detector*, *Eur. Phys. J.* **C 74** (2014) 3184 [arXiv:1407.3146] [INSPIRE].

[9] XENON100 collaboration, E. Aprile et al., *Dark Matter Results from 225 Live Days of XENON100 Data*, *Phys. Rev. Lett.* **109** (2012) 181301 [arXiv:1207.5988] [INSPIRE].

[10] SuperCDMS collaboration, R. Agnese et al., *Search for Low-Mass Weakly Interacting Massive Particles with SuperCDMS*, *Phys. Rev. Lett.* **112** (2014) 241302 [arXiv:1402.7137] [INSPIRE].

[11] SuperCDMS collaboration, R. Agnese et al., *Search for Low-Mass Weakly Interacting Massive Particles Using Voltage-Assisted Calorimetric Ionization Detection in the SuperCDMS Experiment*, *Phys. Rev. Lett.* **112** (2014) 041302 [arXiv:1309.3259] [INSPIRE].

[12] EDELWEISS collaboration, E. Armengaud et al., *A search for low-mass WIMPs with EDELWEISS-II heat-and-ionization detectors*, *Phys. Rev.* **D 86** (2012) 051701 [arXiv:1207.1815] [INSPIRE].

[13] A. Brown, S. Henry, H. Kraus and C. McCabe, *Extending the CRESST-II commissioning run limits to lower masses*, *Phys. Rev.* **D 85** (2012) 021301 [arXiv:1109.2589] [InSPIRE].

[14] G. Angloher et al., *Commissioning run of the CRESST-II dark matter search*, *Astropart. Phys.* **31** (2009) 270 [InSPIRE].

[15] R. Strauss et al., *A detector module with highly efficient surface-alpha event rejection operated in CRESST-II Phase 2*, arXiv:1410.1753 [InSPIRE].

[16] J. Birks, *The Theory and Practice of Scintillation Counting*, Pergamon Press, (1964).

[17] R. Strauss et al., *Energy-dependent light quenching in CaWO$_4$ crystals at mK temperatures*, *Eur. Phys. J.* **C 74** (2014) 2957 [InSPIRE].

[18] G. Angloher et al., *Results from 730 kg days of the CRESST-II Dark Matter Search*, *Eur. Phys. J.* **C 72** (2012) 1971 [arXiv:1109.0702] [InSPIRE].

[19] A. Erb and J.-C. Lanfranchi, *Growth of high-purity scintillating CaWO$_4$ single crystals for the low-temperature direct dark matter search experiments CRESST-II and EURECA*, *Cryst. Eng. Comm.* **15** (2013) 2301.

[20] A. Münster et al., *Radiopurity of CaWO4 crystals for direct dark matter search with CRESST and EURECA*, *JCAP* **05** (2014) 018 [arXiv:1403.5114] [InSPIRE].

[21] R.F. Lang et al., *Electron and Gamma Background in CRESST Detectors*, *Astropart. Phys.* **32** (2010) 318 [arXiv:0905.4282] [InSPIRE].

[22] R.B. Firestone, C.M. Baglin and S. Chu, *Table of isotopes*, Volume **4**, Wiley, (1999).

[23] R.F. Lang et al., *Scintillator Non-Proportionality and Gamma Quenching in CaWO4*, arXiv:0910.4414 [InSPIRE].

[24] C. Cozzini et al., *Detection of the natural alpha decay of tungsten*, *Phys. Rev.* **C 70** (2004) 064606 [nucl-ex/0408006] [InSPIRE].

[25] GEANT4 collaboration, S. Agostinelli et al., *GEANT4: A simulation toolkit*, *Nucl. Instrum. Meth.* **A 506** (2003) 250 [InSPIRE].

[26] J. Allison et al., *Geant4 developments and applications*, *IEEE Trans. Nucl. Sci.* **53** (2006) 270 [InSPIRE].

[27] J. Schmaler, *The CRESST Dark Matter Search – New Analysis Methods and Recent Results*, Ph.D. Thesis TU München, (2010).

[28] G. Angloher et al., *EURECA Conceptual Design Report*, *Physics of the Dark Universe* **3** (2014) 41.

[29] CRESST collaboration, G. Angloher et al., *Probing low WIMP masses with the next generation of CRESST detector*, arXiv:1503.08065 [InSPIRE].